Acta Geodyn. Geomater., Vol. 21, No. 3 (215), 161–173, 2024
DOI: 10.13168/AGG.2024.0015
journal homepage: https://www.irsm.cas.cz/acta

ORIGINAL PAPER

WATER FIELD DISTRIBUTION CHARACTERISTICS AND SLOPE STABILITY UNDER THE EFFECT OF PREFERENTIAL FLOW ON RAINFALL-DRIVEN SEEPAGE

Xinkai HAN [1] *, Rini Asnida ABDULLAH [1], Zuhaila ISMAIL [2], Amber ISLAM [1] and Zhongxiang LU [1]

[1] *Department of Geotechnics and Transportation, Faculty of Civil Engineering, Universiti Teknologi Malaysia, Johor Bahru, Malaysia*
[2] *Department of Mathematical Sciences, Faculty of Science, Universiti Teknologi Malaysia, Johor Bahru, Malaysia*

**Corresponding author's e-mail:* xinkai.han@graduate.utm.my

ARTICLE INFO

Article history:
Received 14 June 2024
Accepted 22 July 2024
Available online 6 August 2024

Keywords:
Preferential flow
Matrix flow
Dual-permeability
Rainfall infiltration condition
Flow

ABSTRACT

This study examines the influence of preferential flow (PF) on seepage under different rainfall infiltration scenarios, addressing a critical gap in current modeling practices, which often overlook the interactive dynamics between matrix flow (MF) and PF domains within soil environments. In this study, an integrated saturated and unsaturated subsurface flow of dual-permeability (DP) model is developed to calculate seepage and slope stability using pore water pressure. This study aims to conduct numerical experiments of shallow landslides induced by rainfall to quantify the temporal and spatial impact of preferential flow on hydrological mechanisms and slope stability. For low-rainfall intensity, the variation in pore water pressure is greater in the MF domain than in the PF domain. 90 % of rainwater infiltrates downward through the MF domain. Water exchange predominantly occurs in the PF domain, as opposed to the MF domain. The factor of safety decreases from 1.61 to 1.55 when comparing before and after rainfall, which reduces by 3.73 %. For high-rainfall intensity, the pore water pressure variation in the PF domain is more pronounced than in the MF domain. The entirety of precipitation infiltration downwards through the PF domain. Water exchange mainly flows from the PF domain to the MF domain. The factor of safety decreases from 1.61 to 1.45 when comparing before and after rainfall, resulting in a reduction of 9.94 %.

1. INTRODUCTION

Landslides are hazardous geological phenomena commonly induced by rainfall in areas characterized by elevated terrain. The integration of hydrological models with the slope stability analysis method enabled the calculation of the factor of safety and the prediction of the duration and magnitude of landslides (Collins and Znidarcic, 2004; Shuin et al., 2012; Wu et al., 2015; Zhu and Xiao, 2020; Roshan et al., 2021). Hydro-mechanical models that integrate both hydraulic and mechanical aspects can consist of two main types: simplified conceptual models (Moonen et al., 2008) and numerical models (Shao et al., 2015, 2018). These hydrological models vary in complexity, which is determined by the research's scale and specific objectives.

PF can be classified into three distinct types: macropore flow, fingered flow, and funneled flow, each characterized by various structural features (Hendrickx and Flury, 2001). In particular, following seismic events such as earthquakes, the occurrence of fractures, cracks, and fissures in seismic landslides facilitates the formation of slip surfaces and enables PF. Consequently, mountainous regions damaged by earthquakes often exhibit an elevated likelihood of landslide reactivation (Zhang et al., 2014). In the event of intense precipitation or snowmelt, PF may manifest as fingered flow, channeled flow, macropore flow, or a combination of these three (Nimmo, 2012; Beven and Germann, 2013; Hu et al., 2019). Each of these PF types influences the variation in suction and the initiation of landslides by rapid infiltration and pressure propagation. Present hydro-mechanical models frequently employ the Darcy-Richards equation or its simplified forms to quantify transient hydrological processes (Ni et al., 2018; Wang et al., 2020; Zhu et al., 2020). However, models that rely on the single-continuum assumption have faced criticism due to their inadequate ability to accurately depict the hydraulic properties of heterogeneous soils (Beven and Germann, 2013).

In slopes characterized by significant heterogeneity, the phenomenon of PF and transport can have a profound impact on subsurface flow patterns and the movement of contaminants (Allaire et al., 2009). A network of interconnected macropores is frequently observed in many soil types, such as forest soil and semiarid land (Zhang et al., 2018). As an illustration, the burrow of an earthworm can expand from the surface level to considerable depths within the soil, similar to the extension capabilities of decomposed plant roots or fissures in the ground

Cite this article as: Han X, Abdullah RA, Ismail Z, Islam A, Lu Z: Water field distribution characteristics and slope stability under the effect of preferential flow on rainfall-driven seepage. Acta Geodyn. Geomater., 21, No. 3 (215), 161–173, 2024. DOI: 10.13168/AGG.2024.0015

(Edwards et al., 1993; Sander and Gerke, 2009; Yu et al., 2019). The activation and hydraulic connection of the self-organizing preferred flow network occur as the soil saturation increases (Nieber and Sidle, 2010). Compared to the soil matrix, the saturated hydraulic conductivity of PF pathways is significantly higher (Shao et al., 2015). A considerable proportion of subsurface stormflow is conveyed by PF pathways (Šimůnek et al., 2003). Rapid PF occurs through local high-permeability zones, including fractures, macropores, and other structures, and then immediately contributes to the generation of high pore water pressures in deep soils (Hardie et al., 2013). Although the Darcy–Richard´s equation is the predominant method utilized in contemporary software programs, it is inadequate for simulating PF, leading to swift infiltration.

To examine how PF affects hydrological processes, simulations of PF and solute transport have been conducted over a range of sizes, encompassing pore-scale, soil column-scale, hillslope-scale, and catchment-scale investigations (Köhne et al., 2009) employing more advanced models such as DP or dual-porosity model (Gerke and van Genuchten, 1993a; Shao et al., 2016), the multi-permeability model (Wu et al., 2004). The DP model is extensively employed due to its well-defined physical concept and robust simulating capabilities (Mein and Larson, 1973; Köhne et al., 2002; Nimmo, 2012; Beven and Germann, 2013; Shao et al., 2015, 2016, 2017, 2018; Zhang et al., 2018; Hu et al., 2019). The DP model assumes that the soil is composed of two-pore domains that interact and overlap. Approaches to calculating PF in micropores or inter aggregate pores range from those invoking Richards' equation (Gerke and van Genuchten, 1993a; Shao et al., 2017), kinematic wave equation (Šimůnek et al., 2003), and Hagen-Poiseuille's equation (Gerke, 2006). The difference assists water transfer between the two domains in pressure gradient (Shao et al., 2015). Despite their demonstrated efficacy in simulating PF, DP models remain absent from coupling seepage and stress models under Pressure controlled infiltration boundary conditions.

The dual-continuum technique necessitates the inclusion of hydraulic parameters, water exchange parameters, and precise boundary conditions for both domains (Chui and Freyberg, 2009). Once the matrix domain is fully saturated, any excess water continues infiltrating through the preferential flow path, further intensifying the water supply along this specific route (Shao et al., 2015). The boundary conditions for both the matrix and preferred flow domains can be converted from the Neumann flux condition to the Dirichlet pressure condition. It is possible to impose distinct standard conditions on the matrix and preferential flow domains, presuming that these domains are defined by two Darcy-Richards equations, respectively (Gerke and van Genuchten, 1993b; Shao et al., 2016, 2018). However, the boundary conditions of the matrix domain and preferential flow domain do not change at the same time during rainfall infiltration. The infiltration process influences the transformation of the preferential flow boundary condition.

In contrast to the limit equilibrium method, the strength reduction method does not require any assumptions regarding the critical failure surface, resulting in similar safety values and identifying the positions of the crucial slip surfaces (Cheng et al., 2007). Quantifying the position, shape, and size of the plastic deformation area determines the slip surface and factor of safety (Borja et al., 2012). Geotechnical engineering tools and numerical models, such as ABAQUS (Dyson and Tolooiyan, 2018) or FLAC 3D (Dyson and Tolooiyan, 2018), have been extensively utilized for the examination of slope stability in the presence of transient hydrological circumstances, such as rainfall (Chowdhury and Flentje, 2002; Oh and Lu, 2015; Wu et al., 2015; Wang et al., 2022).

This study investigates the impact of PF on seepage in various rainfall infiltration situations. It addresses a significant deficiency in existing modeling approaches, frequently neglecting the interaction dynamics between MF and PF domains in soil. The hydrological phenomena of infiltration and pressure propagation are modeled using DP models, which is a research novelty. The objective of this investigation is to quantify the temporal and spatial impact of preferential flow on slope stability, as well as to investigate the underlying hydrological mechanisms of this phenomenon through numerical experiments of shallow landslides induced by rainfall. Firstly, the conversion of infiltration boundary conditions is determined based on the rainfall intensity, equivalent rainfall intensity, and saturated permeability coefficients in the PF and MF domains. This conversion is utilized to estimate the soil's infiltration capacity. Secondly, this research seeks to analyze the coupling of the hydrological mechanisms and solid mechanics that underlie this phenomenon through numerical experiments involving rainfall-induced shallow landslides. Thirdly, a two-dimensional slope model is employed to examine the water content patterns and water exchange, and the slope stability is estimated during different rainfall intensities. The findings shed light on the soil hydraulic properties and the mechanisms involved in mass mobilization due to rainfall in a slope.

2. MATERIALS AND METHODS

2.1. UNSATURATED INFILTRATION MODEL

The DP model posits that the MF and PF domains coexist and overlap within a single representative elementary volume, producing a uniform distribution throughout the modeling network. The water exchange term establishes the connection between MF and PF in the DP model. The water exchange rate is determined by computing the mean hydraulic conductivities of both domains, considering the moisture and pressure conditions in each domain. The combination of the two Richards' equations with a water exchange function defined by the user results in a coupled system of partial differential equations in mathematics (Gerke and van Genuchten, 1993a):

$$\left(\mathrm{C}_f + S_{ef}S_s\right)\frac{\partial H_{pf}}{\partial t} = \frac{\partial}{\partial z}\left(K_f\frac{\partial H_{pf}}{\partial z} + K_f\right) - \frac{\Gamma_w}{w_f} \quad (1)$$

$$\left(\mathrm{C}_m + S_{em}S_s\right)\frac{\partial H_{pm}}{\partial t} = \frac{\partial}{\partial z}\left(K_m\frac{\partial H_{pm}}{\partial z} + K_m\right) + \frac{\Gamma_w}{w_m} \quad (2)$$

where "f" represents the PF domain, while "m" denotes the matrix domain. C_f and C_m are the differential water capacity ($d\theta/dH_p$); S_{ef} and S_{em} are effective saturation of PF domain and matrix domain; H_{pf} and H_{pm} are the pressure heads of two domains; K_f and K_m are the isotropic hydraulic conductivity; S_s is the specific storage; w_f and w_m are the volumetric ratio of the PF domain and MF domain over the total soil volume, and Γ_w is the water exchange term between the two domains. t is time; z is the vertical coordinate (positive upward).

Soil Water Characteristic Curve (SWCC) was proposed to describe the relationship in C, S_e, K, θ, and H_p in unsaturated soil of both domains in unsaturated soil (van Genuchten, 1980). As shown in Equation (3) to Equation (6), these parameters could be specified by the saturated and residual volumetric water content θ_s and θ_r, as well as constants of a, n, m, and l.

$$\theta = \theta_r + \frac{(\theta_s - \theta_r)}{\left(1+|aH_p|^n\right)^m} \quad (3)$$

$$S_e = \frac{1}{\left(1+|aH_p|^n\right)^m}, m = 1 - \frac{1}{n} \quad (4)$$

$$C = \frac{(\theta_s - \theta_r)mna|aH_p|^{n-1}}{\left(1+|aH_p|^n\right)^{m+1}} \quad (5)$$

$$K = \mathrm{K}_s S_e^{\,l}\left[1 - \left(1 - S_e^{\frac{1}{m}}\right)^m\right]^2 \quad (6)$$

where K_s is the saturated hydraulic conductivity (m/s), α, n, m, and l are the fitting parameters of the soil-water characteristic curve. S_e is effective saturation, K_r is relative permeability or the unsaturated water conductivity (m/s).

The transfer term Γ_w is the water exchange rate in the difference of pressure head both domains (Gerke and van Genuchten, 1993a):

$$\Gamma_w = a_w K_a\left(H_{pf} - H_{pm}\right) \quad (7)$$

where a_w is the first transfer effective water transfer coefficient for fluid. The hydraulic conductivities K_a is elevated as the mean function of hydraulic conductivity between MF domain and PF domain (Shao et al., 2015):

$$K_a = \frac{K_f + K_m}{2} \quad (8)$$

Since C and K are both variables related to pressure head H_p, Equations (1) and (2) are second-order nonlinear PDEs, which is solved by numerical methods under certain assumptions.

The volumetric ratio of the PF domain and matrix domain sum up to 1:

$$w_f + w_m = 1 \quad (9)$$

The total water content of the soil is the weighted average of the water contents of the two domains

$$\theta = w_f\theta_f + w_m\theta_m \quad (10)$$

The same holds for the total saturated hydraulic conductivity of the soil:

$$\mathrm{K}_s = w_f\mathrm{K}_{sf} + w_m\mathrm{K}_{sm} \quad (11)$$

where K_{sf} and K_{sm} are saturated hydraulic conductivity of the PF domain and MF domain, respectively.

The weighted average of the effective saturation of the two domains can be expressed by (Shao et al., 2016):

$$S_{ew} = w_f S_{ef} + w_m S_{em} \quad (12)$$

2.2. SOIL INFILTRATION CAPACITY MODEL

By introducing complementary smoothing functions α and β, the soil infiltration capacity f_{cm} and f_{cf} of general mixed boundary condition in the two domains are enhanced and defined in COMSOL (Chui and Freyberg, 2009):

$$f_{cm} = \alpha R + \beta\frac{K_{sm}}{L}\left(H_w - \frac{p_m}{\rho g}\right) \quad (13)$$

$$f_{cf} = \alpha R + \beta\frac{K_{sf}}{L}\left(H_w - \frac{p_f}{\rho g}\right) \quad (14)$$

where H_w is the water depth of surface; A coupling length scale $L = 0.001$ m.
α can be expressed by:

$$\alpha = \begin{cases} 1, & p < 0 \\ 0, & p \geq 0 \end{cases} \quad (15)$$

β is defined as

$$\beta = 1 - \alpha \quad (16)$$

The general boundary condition simplifies to a Neumann condition when α=1 and β=0, and to a Dirichlet condition when $\frac{K_{sm}}{L}$ and $\frac{K_{sf}}{L}$ are infinite (α=0 and β=1). Therefore, this mixed boundary condition represents a solution-dependent switch between Neumann and Dirichlet conditions by specifying complementary smoothing functions.

2.3. BOUNDARY CONDITIONS OF DP MODEL

The soil infiltration capacity f_{cm} and f_{cf} are determined by the pressure head at the surface (zero or higher depending on the increasing runoff H_w) and the pressure head in the cell below. The rainfall infiltration process consists of two sequential steps. Firstly, infiltration occurs before runoff generation in the early rainfall event. The rainfall intensity R is less than the

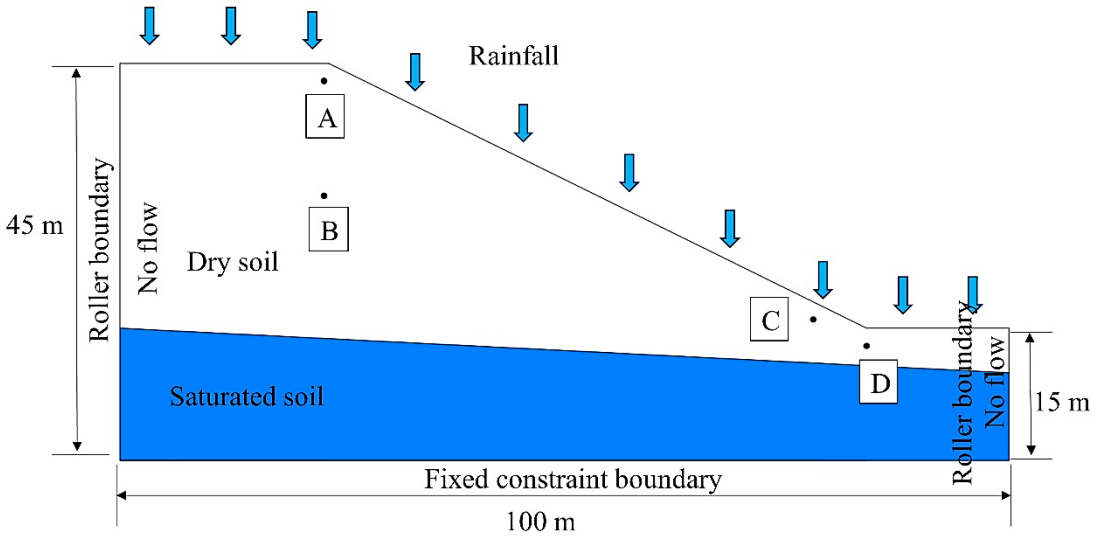

Fig. 1 The geometry of the slope and the boundary conditions.

saturated hydraulic conductivity K_{sm} of subsurface MF, which is treated as a flow boundary condition at the slope surface for calculating subsurface flow. The infiltration rates of both domains are initially equal to rainfall intensity *R*.

$$\mathrm{R} = \mathrm{I} = \mathrm{I}_m = \mathrm{I}_f \tag{17}$$

Secondly, when rainfall intensity R is greater than the saturated hydraulic conductivity K_{sm} of MF but is less than the saturated hydraulic conductivity K_{sf} of PF. The infiltration rate I_m is equal to soil infiltration capacity f_{cm}. Then, the runoff occurs at the top of the MF domain, transforming from the flow boundary condition to the pressure head condition. However, the flow boundary condition can still be applied in PF. The excess water is equivalent to infiltrating PF from the surface and is treated as equivalent rainfall intensity. The equivalent rainfall intensity of PF is expressed by

$$\mathrm{R}_f = \frac{R - \mathrm{w}_m \mathrm{I}_m}{\mathrm{w}_f} \tag{18}$$

When equivalent rainfall intensity R_f is less than the saturated hydraulic conductivity K_{sf} of PF. The actual infiltration rate I_f can be expressed by:

$$I_f = \mathrm{R}_f \tag{19}$$

When equivalent rainfall intensity R_f exceeds the saturated hydraulic conductivity K_{sf} of PF, runoff generate on the surface. The infiltration rate I_f is equal to soil infiltration capacity f_{cf}. The boundary conditions of both domains transform into pressure head condition, which is determined by the ponding depth.

2.4. DRUCKER–PRAGER YIELD CRITERION

The Drucker–Prager yield criterion is used to describe the yield condition, which can be expressed as

$$F = \sqrt{J_2} + mI_1 - n \tag{20}$$

where J_2 is the second invariant of the stress deviator tensor, I_1 is the first invariant of the effective stress tensor. m and n are two material constants.

The mechanical calculation uses the linear elastic model with the Drucker-Prager criterion, matching the Mohr-Coulomb criterion; the parameters are

$$m = \frac{tan(\varphi)}{\sqrt{9+12\,tan^2(\varphi)}} \tag{21}$$

$$n = \frac{3c}{\sqrt{9+12\,tan^2(\varphi)}} \tag{22}$$

where c is the soil cohesion, and φ is the internal friction angle of the soil.

2.5. SLOPE GEOMETRY OF NUMERICAL MODEL

The suggested test slope is 100 m long, with a height of 45 m, a toe height of 15 m, and a slope angle 26 degrees. The following are the boundary conditions that govern the subsurface flow model. The surface is atmospheric. The left, right, and bottom sides have no flow boundaries. The left and right sides specify pressure heads to simulate variable groundwater tables, as shown in Figure 1. The soil water characteristics curve (SWCC) is typically obtained through a pressure plate test. The VG fitting parameters are obtained by fitting the VG Equation (3) to the experimental data from the SWCC test.

The residual soil sample hydraulic parameters are presented in Table 1.

Table 1 Summary of parameters.

Parameter name	Symbol	Residual Soil	Units
Dry unit weight	ρ_s	14.3	kN/m^3
Saturated hydraulic conductivity	K_s	7.91×10^{-6}	m/s
Saturated hydraulic conductivity of PF domain	K_{sf}	7.25×10^{-5}	m/s
Saturated hydraulic conductivity of MF domain	K_{sm}	7.25×10^{-7}	m/s
Young's modulus	E	10^5	kPa
Poisson's ratio	V	0.35	
Effective cohesion	c	15	kPa
Friction angle	phi	26	°
Saturated water content	θ_s	0.57	
Residual water content	θ_r	0.08	
VG fitting parameter	a	0.36	
VG fitting parameter	n	1.37	
VG fitting parameter	l	0.5	

This study simulates two rainfall intensities: low-intensity rainfall 2 mm/h lasting 240 h, and high-intensity rainfall 20 mm/h lasting for 24 h. These events are being investigated to analyze the impact on several factors, such as effective saturation, water exchange rate, pore water pressure, infiltration rate, boundary pressure, and slope stability.

3. RESULTS

3.1. EFFECTIVE SATURATION ANALYSIS

The study area examines the distribution of soil effective saturation, taking into account the influence of both MF domain and PF domain under varying rainfall intensities., is depicted in Figure 2. To improve the convergence of the DP model, the initial condition of effective saturation is obtained from the stationary analysis. During the initial phase, the soil at the bottom of the slope toe is saturated from a height of 15 meters on the left to a height of 10 meters on the right. Besides, matric suction affects soil saturation. Soils beyond this level, however, remain unsaturated. In two rainfall intensity conditions, low- and high-rainfall intensity, the wetting front develops parallel to the surface and progresses downhill in the DP model. The rainwater usually reaches the slope's toe initially, where it encounters the groundwater table, leading to the ongoing enlargement of the saturated region in Figure 2.

For the low-intensity rainfall in Figure 2, the variations of effective saturation of surface soil mass primarily occur in the MF domain. In contrast, the PF domain exhibits a high saturation permeability coefficient, leading to minimal changes in saturation. After 120 hours of rainfall, the wetting front in the PF area has reached the groundwater level, resulting in an overall rise in the amount of moisture content in the PF domain. Nevertheless, there is no significant rise in groundwater levels due to low rainfall intensity. During 240 hours of rainfall, the water level at the base of the MF domain experiences a modest increase. For high-intensity rainfall in Figure 2, it is observed that soil saturation of MF domain increased significantly within 1.1-meter thickness at the surface. Moreover, as equivalent rainfall intensity increases, the effective saturation of the PF domain substantially rises. As a result of rapid infiltration, prolonged rainfall lasting 12 hours causes the groundwater level in the PF domain to reach the surface at the toe of the slope. After 24 hours of rainfall, the soil at the base of the hill had been completely saturated. The MF domain mostly governs the infiltration of the low-rainfall intensity, whereas the infiltration of the high-rainfall intensity is primarily governed by the PF domain by comparing the two rainfall situations. The infiltration depth of the PF domain surpasses that of the pore domain. Rainwater initially reaches the groundwater level at the slope toe, and subsequently expands the saturated area continuously. By analyzing the variations in effective saturation for two rainfall intensities, the groundwater levels in both domains consistently rise in unison.

3.2. PORE WATER PRESSURE ANALYSIS

The increase of soil saturation may lead to variations of pore water pressure between initial condition and continuous rainfall, respectively, as illustrated in Figure 3. Following the law of saturation change, the pore water pressure in soils at the shallow surface and the toe of the slope increased substantially, with the most pronounced change occurring at the slope toe; The pore pressure remains negative and unaltered at the depths of the slope.

To further examine the law variation of pore water pressure in both domains during rainfall, the vulnerable points A, B, C and D are plotted, as indicated in Figure 1. These monitoring points are strategically positioned at four different locations within the slope, namely the shoulder/crest (Point A), deep region (Point B), left side of slope toe (Point C), and below slope toe (Point D). For low-rainfall intensity, the pore water pressure is negative at four points between the PF domain and MF, suggesting that

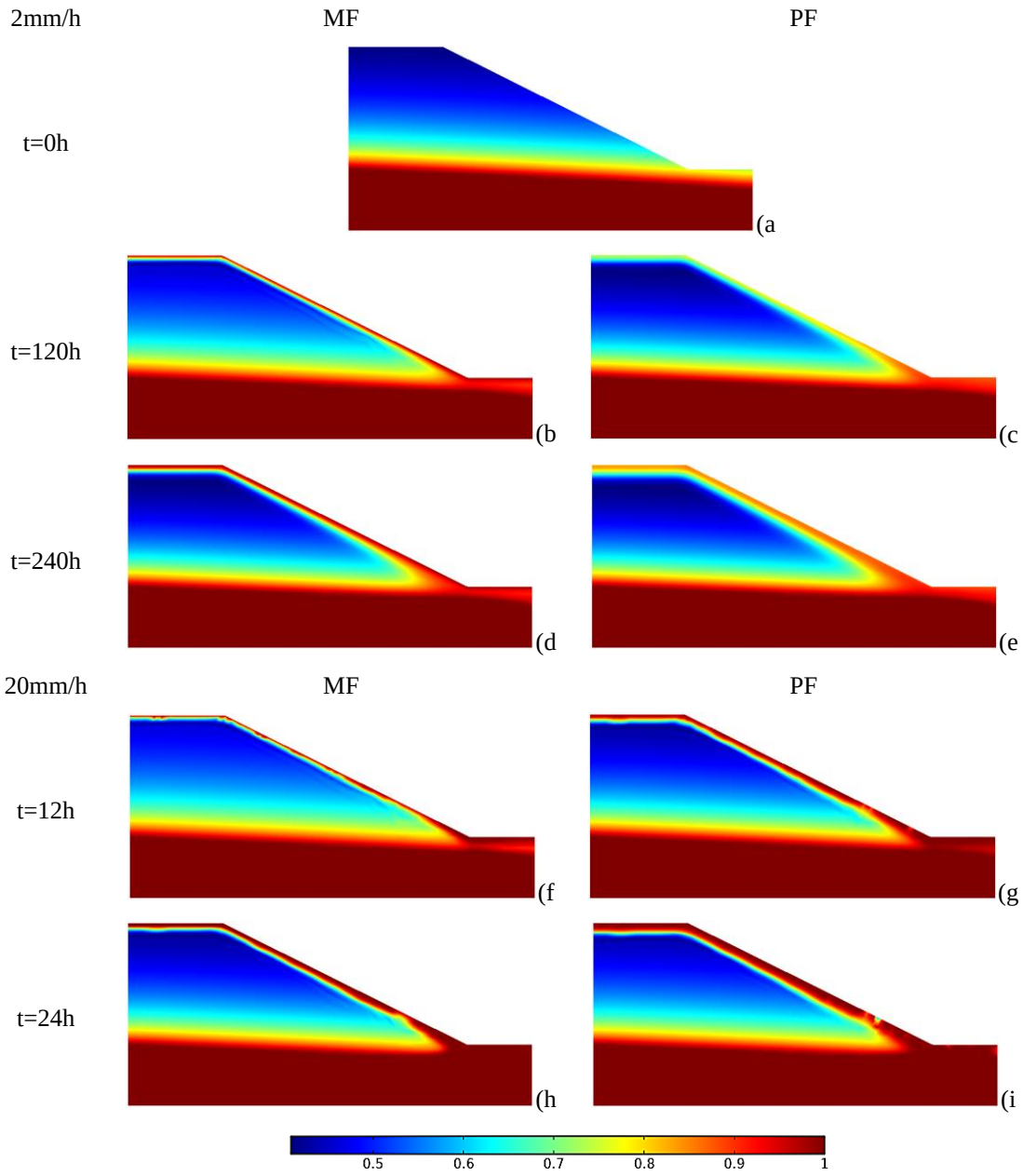

Fig. 2 Variation of effective saturation during different rainfall intensities.

soils at these points are unsaturated, as shown in Figure 4. It is observed that the pore water pressure has the most prominent increase at point A. Moreover, the difference is most significant between the PF and MF domains. The pore pressure at point C and point D of the slope toe experience a certain degree of increase, while the pore pressure at point B (deep in the slope) remains essentially unchanged with continuous rainfall. For high-rainfall intensity, the pore water pressure is positive after 16 hours of rainfall at point D, and then the soil is saturated. Soils at the other three points are all unsaturated. The most significant increase of the pore water pressure is observed at point A. Furthermore, the disparity is most pronounced when transitioning from the PF domain to the MF domain. As rainfall intensity increases, the difference between the PF and MF domains exhibits an increasing trend.

3.3. INFILTRATION RATE AND BOUNDARY PRESSURE ANALYSIS

When the rainfall intensity is 2 mm/h, the infiltration rates in the MF domain and PF domain are equal to the rainfall intensity, as shown in Figure 5. Different amounts of pore water pressure rose in both domains, but the pore water pressure in the MF

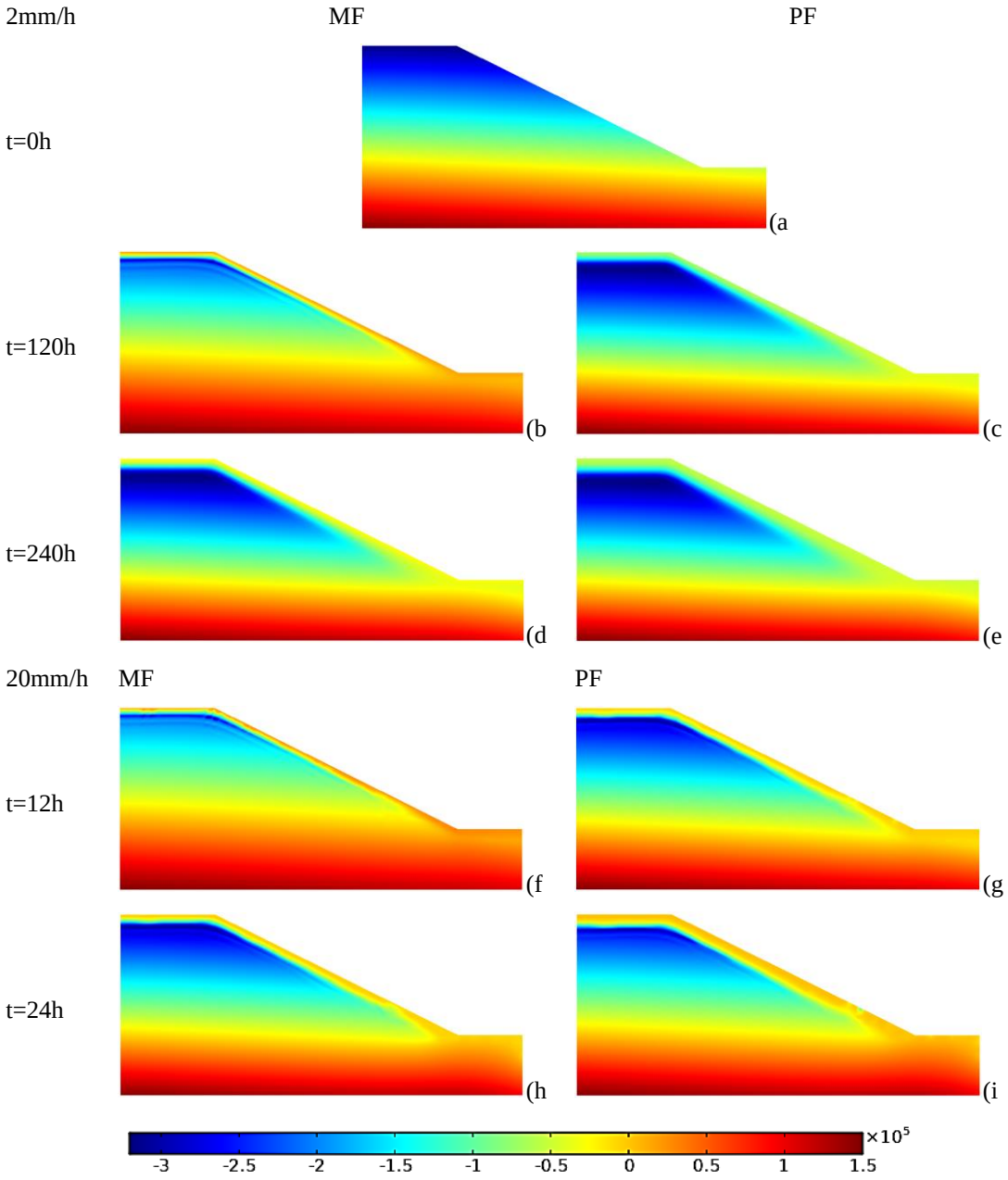

Fig. 3 Pore water pressure contours of DP at different rainfall intensities.

domain is closer to 0, as shown in Figure 6. At a rainfall intensity of 20 mm/h, the MF domain rapidly becomes completely saturated after 2 hours rainfall, as indicated in Figure 5. Consequently, the boundary condition shifts from flow boundary to pressure boundary, as indicated in Figure 6. Moreover, all surplus water is directed towards the PF domain and seeps farther down, resulting in a progressive rise in the intensity of rainfall inside the PF domain. It is observed that the infiltration rate begins to increase progressively as the equivalent rainfall intensity increases. After 24 hours of rainfall, the infiltration rate of PF domain increases to 4.624×10^{-5} m/s. Furthermore, the PF domain's rainfall intensity can be determined using Equation (12), whose value is 4.623×10^{-5} m/s. Therefore, the error of the numerical calculation is ureinimal. The pore water pressure is measured at 0.11 kPa on the surface after 2 hours of rainfall. The infiltration pressure boundary condition indicated that the specified ponding depth is 0.01 m, corresponding to a calculated pressure of 0.1 kPa. These two values show a high level of concordance and agreement. The preferential domain's saturated permeability coefficient is so high that it will not attain saturation even if all excess water from the MF domain flows into it. A progressive increase in pore water pressure is observed in the PF domain as the equivalent rainfall intensity rises.

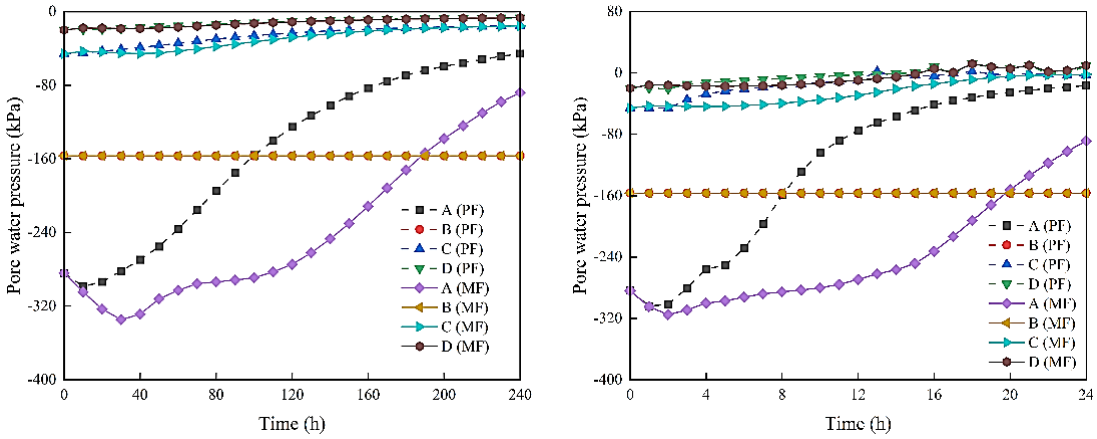

(a 2mm/h (b 20mm/h

Fig. 4 Vulnerable points of pore water pressure contours of DP at different rainfall intensities.

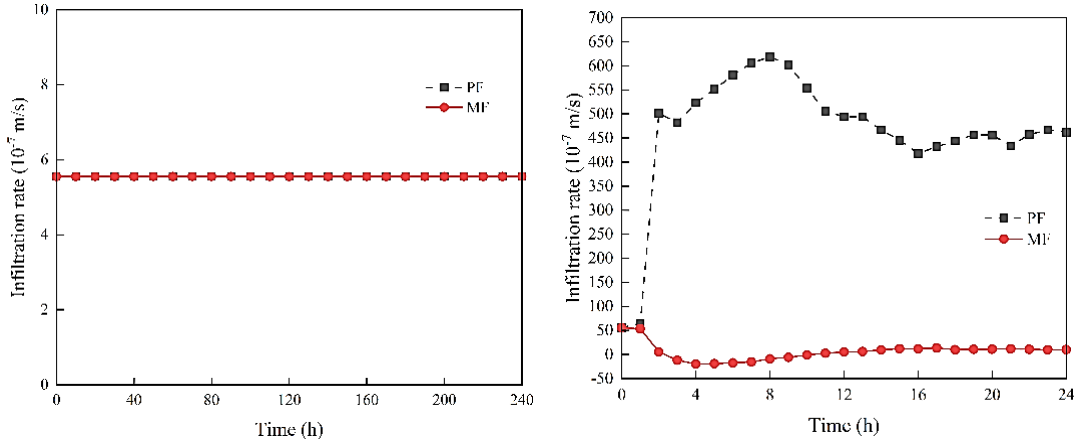

(a 2mm/h (b 20mm/h

Fig. 5 Infiltration rate of DP at different rainfall intensities.

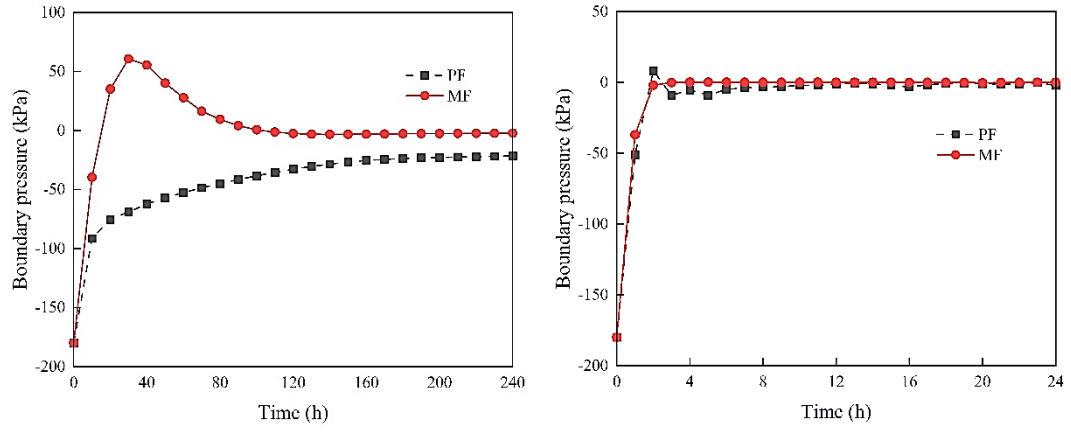

(a 2mm/h (b 20mm/h

Fig. 6 Boundary pressure of DP at different rainfall intensities.

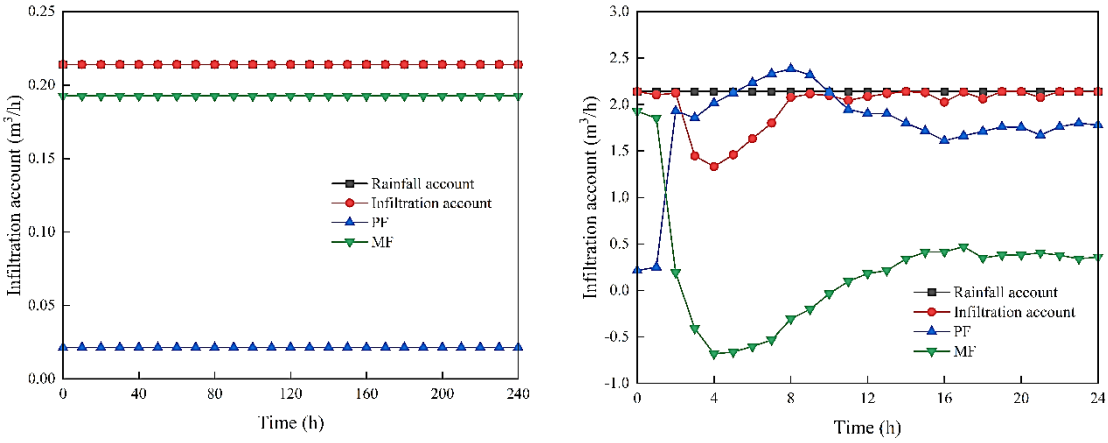

(a 2mm/h (b 20mm/h

Fig. 7 Rainfall account of DP at different rainfall intensities.

3.4. INFILTRATION AMOUNT ANALYSIS

To calculate the infiltration account of the PF domain and MF domain at different times, the boundary of the study area is performed line integration, and the longitudinal thickness of the two-dimensional slope model is assumed to be 1 m. When the rainfall intensity is 2 mm/h, rainwater mainly infiltrates downward through the MF domain, as indicated in Figure 7. The total infiltration amount is equal to the rainfall intensity. When the rainfall intensity is 20 mm/h, all rainwater penetrates into the PF domain and MF domain before 2 hours, as indicated in Figure 7. The excess water cannot be absorbed into the PF domain within 2 to 10 hours. Runoff occurs on the surface because high-intensity rainfall cannot wholly pass through saturated areas on the shallow surface. The part of excess water infiltrates into the PF domain, which causes an increase of equivalent rainfall. The rainfall amount is approximately equal to the amount of infiltration after 8 hours. It is obtained that the amount of rainfall is 51.4 m^3. The total infiltration account of 2 mm/h lasting for 240 h is 51.4 m^3, and the entire infiltration account of 20 mm/h lasting for 24 h is 49.86 m^3. Therefore, the total infiltration account of 2 mm/h lasting for 240 h is slightly larger than that of 20 mm/h lasting for 24 h.

3.5. WATER EXCHANGE ANALYSIS

The water exchange rate between the MF domain and PF domain of the DP model is depicted in Figure 8. The principal direction of water exchange at a precipitation intensity of 2 mm/h is from the MF domain to the PF domain. The water exchange rate gradually decreases as the MF domain and PF infiltration depth grows. The PF domain exhibits a greater penetration depth in the slope's lower portion than the MF domain. As a result of the rapid infiltration rate in the PF domain, the saturation of the mass in the PF domain, where the wetting peak surpasses the MF domain, is slightly higher than that in the MF domain.

Consequently, water exchange is from the PF domain to the MF domain in this area. Most water exchange infiltrates from the PF domain to the MF domain when there is a 20 mm/h rainfall. The amount of water exchange that flows into the MF domain quickly rises as the PF domain rainfall intensity and infiltration depth gradually rise. Water moves from the MF domain to the PF domain in the upper part of the slope, where the MF domain is fully saturated. Besides, the most significant difference of water exchange rate is observed on the shallow surface. The water exchange rate in both domains is lower during low-rainfall intensity compared to high-rainfall intensity periods.

3.6. SLOPE STABILITY ANALYSIS

The factor of safety is calculated using the strength reduction method in this study, using two distinct levels of rainfall intensity. The linear elastic model with the Drucker-Prager criterion is used for the mechanical calculation, which matches the Mohr-Coulomb criterion. The parameter sweep method in COMSOL Multiphysics facilitated the quick assessment of how different parameter values affected the calculated results. Effective cohesion *c* and friction angle *phi* are required as input parameters. As shown in Figure 9, the slope initial factor of safety of varying rainfall accounts equals 1.61. When the rainfall intensity is 2 mm/h lasting for 240 hours, the slope factor of safety reduces to 1.55 after 4.8 m^2 rainfall account. Furthermore, the decreasing trend factor of safety is slightly slower. The factor of safety is reduced by 3.73 % compared to the initial factor of safety. When the rainfall intensity is 20 mm/h, lasting for 24 hours, the factor of safety for the slope decreases to 1.45 after rainfall of 4.8 m^2. However, the

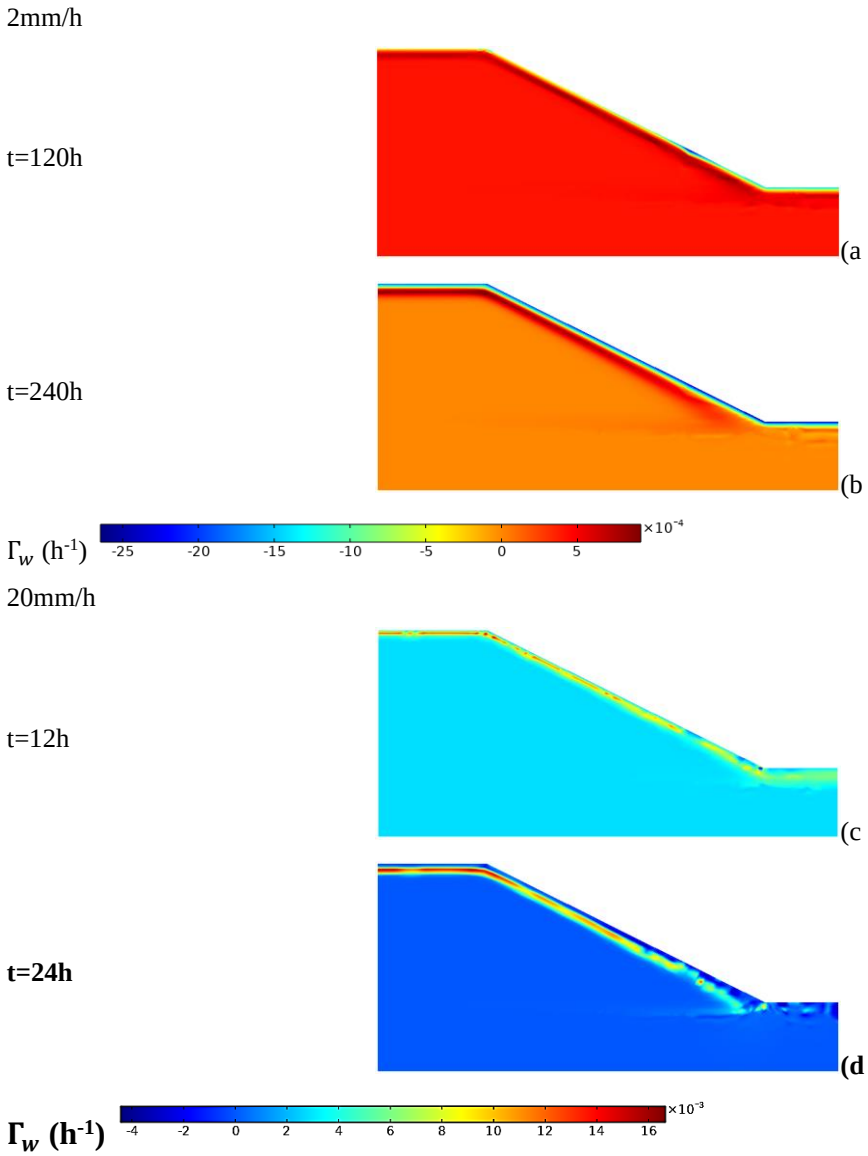

Fig. 8 Water exchange rate distribution of DP.

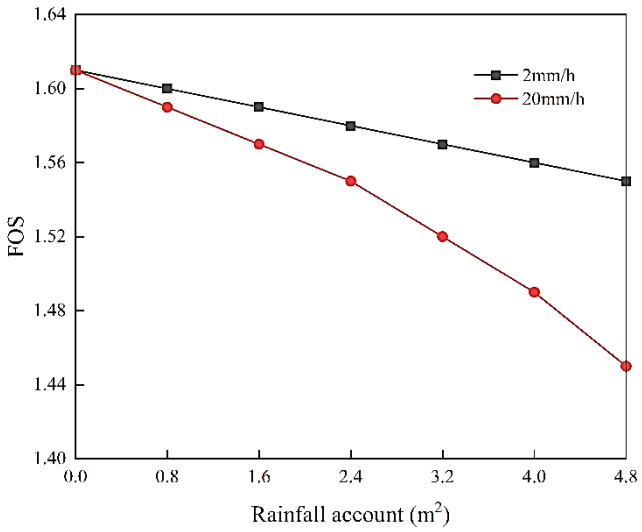

Fig. 9 Variation of FOS during different rainfall intensities.

Table 2 Different water exchange coefficients in previous literature.

Parameters	β	a_l (cm)	γ_w	a_w (cm^{-2})	References
Sandy loam soil	15	0.3	0.4	66.67	Kodešová, R et al. (Kodešová et al., 2005)
Sandy loam soil	0.54	4.85	0.001	1.2×10^{-5}	Arora et al. (Arora et al., 2011)
Clay				2×10^{-5}	Shao, W et al. (Shao et al., 2015)
Clay	3	0.38	0.4	8.31	Aguilar-López et al. (Aguilar-López et al., 2020)
	3	2.449	0.4	2×10^{-5}	This study

rate of decline is relatively rapid. The factor of safety decreases by 9.94 % compared with the initial factor of safety.

4. DISCUSSION

The pore water pressure value is significant in the DP model's fluid-solid coupling. Two methods exist to estimate pore water pressure based on seepage and stress. The average pore water pressure estimated the pore-network modeling of (two-phase) flow in porous media (Korteland et al., 2010). Moreover, the PF pore water pressure is used to calculate the stress in the DP model (Shao et al., 2015). The specific situation determines the value of pore water pressure because the initial hydrological conditions are calculated from the steady state of previous rainfall. Therefore, this study employs the average pore water pressure to calculate the stress.

Physical measurements make it extremely difficult to estimate the water exchange coefficient. The water exchange parameterization employed in this study was compared to that of earlier investigations in Table 2. The Equation (8) is most widely used (Gerke and van Genuchten, 1993b). Köhne and Mohanty (2005) showed how chlortoluron naturally moves through the soil profile. Arora et al. (2011) estimated parameters for multidomain flow models in soil columns with varying macropore densities. These preferential flow systems can be modeled as the dual-permeability porous medium by modifying the fracture domain's 2-D formulation, initial conditions, and mass exchange function (Aguilar-López et al., 2020). This study ignores the impact of coatings on permeability, as well as Köhne and Mohanty (2005), Arora et al. (2011), and Aguilar-López et al. (2020).

This study examines the influence of PF on seepage in different rainfall infiltration scenarios. It tackles a notable inadequacy in current modeling methods, which often overlook the interconnected dynamics between MF and PF domains in soil. This study tries to figure out how PF affects slope stability over time and space, as well as how it works on a hydrological mechanism, by simulating rainfall-induced shallow landslides numerically. This method has substantial implications for precisely identifying the hazardous area on a large catchment scale and precisely disseminating warning information to the hazardous areas. While a linear-elastic model is used to analyze the stress distribution and evaluate failure, it should be noted that the results do not indicate any occurrence of plastic deformation after failure. Our findings suggest that additional research is necessary to address topics such as the influence of plastic deformation following failure on slope stability.

5. CONCLUSION

The coupling DP model is used to simulate the subsurface hydrological effects of PF. The impact of precipitation events on the DP model is investigated in numerical experiments. The investigation concentrated on two classifications of rainfall events: low-intensity, long-duration rainfall and high-intensity, short-duration rainfall. The cumulative precipitation from both rainfall events is equivalent. The following conclusions can be drawn:

1. The conversion of derived infiltration boundary conditions in the PF domain and the MF domain is related to the rainfall intensity, the equivalent rainfall intensity, and the saturated permeability coefficients of both domains. The resulting pressure boundary condition is compared to example models in existing literature, and the calculation results demonstrate strong consistency with the conclusions drawn in earlier investigations.
2. At a rainfall intensity of 2 mm/h, the infiltration account of both domains is equivalent to the rainfall account. 90 % of rainwater infiltrates downward through the MF domain, resulting a significant change in moisture content in this domain. Therefore, infiltration is mainly controlled by the MF domain. When the rainfall intensity reaches 20 mm/h, all the rainwater seeps into the PF domain. The infiltration rate of the PF domain significantly exceeds that of the MF domain. Furthermore, infiltration is primarily governed by the PF domain, which accounts for the substantial variation in moisture content.
3. Water exchange mainly flows from the MF domain to the PF domain for low-rainfall intensity. Compared to the MF domain, the PF domain exhibits a greater penetration depth in the lower portion of the slope. A thimbleful of water exchange flows from the MF domain to the PF domain in the lower portion of the slope. For high-rainfall intensity, water exchange mainly flows from the PF domain to the MF domain

because the saturation area of the MF domain occurs on the shallow surface. Moreover, water exchange occurs from the PF domain to the MF domain for nearly the entire spectrum of slope infiltration depth. In both domains, the water exchange rate is lower during periods of low rainfall intensity than in high rainfall intensity.

4. It is obtained that when the rainfall intensity is 2 mm/h and lasts for 240 hours, the slope's factor of safety decreases to 1.55 after a cumulative rainfall of 4.8 m^2 through the strength reduction method. The factor of safety reduces by 3.73 % compared to the initial factor of safety. When the rainfall intensity is 20 mm/h and lasts for 24 hours, the slope's factor of safety reduces to 1.45 after a rainfall of 4.8 m^2. The factor of safety decreases by 9.94 % compared to the initial factor of safety. The decline rate of the factor of safety of high-rainfall intensity is faster than that of low-rainfall intensity under the same rainfall account.

AUTHOR CONTRIBUTION

Xinkai Han: data curation, formal analysis, methodology, software, writing—original draft, review and editing.
Rini Asnida Abdullah: investigation, methodology, supervision, funding acquisition.
Zuhaila Ismail: software, investigation, methodology, supervision.
Amber Islam: formal analysis, software, investigation.
Zhongxiang Lu: formal analysis, software, investigation.

ACKNOWLEDGMENTS

The authors would like to acknowledge the Universiti Teknologi Malysia for the financial research support under UTM Fundamental Research Grant (UTMFR: Q.J130000.3822.22H78).

REFERNCES

Aguilar-López, J.P., Bogaard, T. and Gerke, H.H.: 2020, Dual-permeability model improvements for representation of preferential flow in fractured clays. Water R**e**sour. Res., 56, 8, 1–20. DOI:10.1029/2020WR027304

Allaire, S.E., Roulier, S. and Cessna, A.J.: 2009, Quantifying preferential flow in soils: A review of different techniques. J. Hydrol., 378, 1–2, 179–204. DOI: 10.1016/j.jhydrol.2009.08.013

Arora, B., Mohanty, B.P. and McGuire, J.T.: 2011, Inverse estimation of parameters for multidomain flow models in soil columns with different macropore densities. Water Resour. Res., 47, 4, 1–17. DOI:10.1029/2010WR009451

Beven, K. and Germann, P.: 2013, Macropores and water flow in soils revisited. Water Resour. Res., 49, 6, 3071–3092. DOI:10.1002/wrcr.20156

Borja, R.I., White, J.A., Liu, X. and Wu, W.: 2012, Factor of safety in a partially saturated slope inferred from hydro-mechanical continuum modeling. Int. J. Numer. Anal. Methods Geomech., 36, 236–248. DOI: 10.1002/nag.1021

Cheng, Y.M., Lansivaara, T. and Wei, W.B.: 2007, Two-dimensional slope stability analysis by limit equilibrium and strength reduction methods. Comput. Geotech., 34, 3, 137–150. DOI: 10.1016/j.compgeo.2006.10.011

Chowdhury, R. and Flentje, P.: 2002, Uncertainties in rainfall-induced landslide hazard. Q. J. Eng. Geol. Hydrogeol., 35, 61–69. DOI: 10.1144/qjegh.35.1.61

Chui, T.F.M. and Freyberg, D.L.: 2009, Implementing hydrologic boundary conditions in a multiphysics model. J. Hydrol. Eng., 14, 12, 1374–1377. DOI: 10.1061/(ASCE)HE.1943-5584.0000113

Collins, B.D. and Znidarcic, D.: 2004, Stability analyses of rainfall induced landslides. J. Geotech. Geoenviron. Eng., 130, 4, 362–372. DOI:10.1061/(asce)1090-0241(2004)130:4(362)

Dyson, A.P. and Tolooiyan, A.: 2018, Optimisation of strength reduction finite element method codes for slope stability analysis. Innov. Infrastruct. Solut., 3, 1, 1–12. DOI:10.1007/s41062-018-0148-1

Edwards, W.M., Shipitalo, M.J., Owens, L.B. and Dick, W.A.: 1993, Factors affecting preferential flow of water and atrazine through earthworm burrows under Continuous no-till corn. J. Environ. Qual., 22, 3, 453–457. DOI: 10.2134/jeq1993.00472425002200030008x

Mein, R.G. and Larson, G.L.: 1973, Modeling infiltration during a steady rain. Water Resour. Res., 9, 2, 384–394. DOI: 10.1029/WR009i002p0038

van Genuchten, M.: 1980, A closed-form equation for predicting the hydraulic conductivity of unsaturated soils. Soil Sci. Soc. Am. J., 44, 5, 892–898. DOI: 10.2136/sssaj1980.03615995004400050002x

Gerke, H.H.: 2006, Preferential flow descriptions for structured soils. J. Plant Nutr. Soil Sci., 169, 3, 382–400. DOI: 10.1002/jpln.200521955

Gerke, H.H. and van Genuchten, M.T.: 1993a, Evaluation of a first-order water transfer term for variably saturated dual-porosity flow models. Water Resour. Res., 29, 4, 1225–1238. DOI: 10.1029/92WR02467

Gerke, H.H. and van Genuchten, M.T: 1993b, A dual-porosity model for simulating the preferential movement of water and solutes in structured porous media. Water Resour. Res., 29, 2, 305–319. DOI: 10.1029/92WR02339

Hardie, M., Lisson, S., Doyle, R. and Cotching, W.: 2013, Determining the frequency, depth and velocity of preferential flow by high frequency soil moisture monitoring. J. Contam. Hydrol., 144, 1, 66–77. DOI: 10.1016/j.jconhyd.2012.10.008

Hendrickx, J.M. and Flury, M.: 2001, Uniform and preferential flow mechanisms in the vadose zone. National Academy Press, 149–188.

Hu, H., Wen, J., Peng, Z., Tian, F., Tie, Q., Lu, Y. and Khan, M.Y.A.: 2019, High-frequency monitoring of the occurrence of preferential flow on hillslopes and its relationship with rainfall features, soil moisture and landscape. Hydrol. Sci. J., 64, 11, 1385–1396. DOI: 10.1080/02626667.2019.1638513

Kodešová, R., Kozák, J., Šimůnek, J. and Vacek, O.: 2005, Single and dual-permeability models of chlorotoluron transport in the soil profile. Plant Soil Environ., 51, 7, 310–315. DOI: 10.17221/3591-pse

Köhne, J.M., Köhne, S. and Gerke, H.H.: 2002, Estimating the hydraulic functions of dual-permeability models from bulk soil data. Water Resour. Res., 38, 7, 26-1-26–11. DOI: 10.1029/2001wr000492

Köhne, J.M., Köhne, S. and Šimůnek, J.: 2009, A review of model applications for structured soils: a) Water flow and tracer transport. J. Contam. Hydrol., 104, 1–4, 4–35. DOI: 10.1016/j.jconhyd.2008.10.002

Köhne, J.M. and Mohanty, B.P.: 2005, Water flow processes in a soil column with a cylindrical macropore: Experiment and hierarchical modeling. Water Resour. Res., 41, 3. DOI: 10.1029/2004WR003303

Korteland, S., Bottero, S., Hassanizadeh, S.M. and Berentsen, C.W.J.: 2010, What is the correct definition of average pressure? Transport Porous Med., 84, 1, 153–175. DOI: 10.1007/s11242-009-9490-2

Moonen, P., Carmeliet, J. and Sluys, L.J.: 2008, A continuous-discontinuous approach to simulate fracture processes in quasi-brittle materials. Philos. Mag., 88, 28–29, 3281–3298. DOI: 10.1080/14786430802566398

Ni, J.J., Leung, A.K., Ng, C.W.W. and Shao, W.: 2018, Modelling hydro-mechanical reinforcements of plants to slope stability. Comput. Geotech., 95, 99–109. DOI: 10.1016/j.compgeo.2017.09.001

Nieber, J.L. and Sidle, R.C.: 2010, How do disconnected macropores in sloping soils facilitate preferential flow? Hydrol. Process., 24, 12, 1582–1594. DOI: 10.1002/hyp.7633

Nimmo, J.R.: 2012, Preferential flow occurs in unsaturated conditions. Hydrol. Process., 26, 5, 786–789. DOI:10.1002/hyp.8380

Oh, S. and Lu, N.: 2015, Slope stability analysis under unsaturated conditions: Case studies of rainfall-induced failure of cut slopes. Eng. Geol., 184, 96–103. DOI: 10.1016/j.enggeo.2014.11.007

Roshan, M.J., Rashid, A.S.A., Wahab, N.A., Hezmi, M.A., Jusoh, S.N. and Azmi, M.: 2021, Stability of railway embankment in saturated and unsaturated conditions. IOP Conf. Ser. Mater. Sci. Eng., 1153, 1, 012007. DOI: 10.1088/1757-899x/1153/1/012007

Sander, T. and Gerke, H.H.: 2009, Modelling field-data of preferential flow in paddy soil induced by arthworm burrows. J. Contam. Hydrol., 104, 1–4, 126–136. DOI: 10.1016/j.jconhyd.2008.11.003

Shao, W., Bogaard, T.A., Bakker, M. and Greco, R.: 2015, Quantification of the influence of preferential flow on slope stability using a numerical modelling approach. Hydrol. Earth Syst. Sci., 19, 5, 2197–2212. DOI: 10.5194/hess-19-2197-2015

Shao, W., Bogaard, T., Su, Y. and Bakker, M.: 2016, Coupling a 1D Dual-permeability model with an infinite slope stability approach to quantify the influence of preferential flow on slope stability. Procedia Earth Planet. Sci., 16, 0, 128–136. DOI: 10.1016/j.proeps.2016.10.014

Shao, W., Ni, J., Leung, A.K., Su, Y. and Ng, C.W.W.: 2017, Analysis of plant root-induced preferential flow and pore-water pressure variation by a dual-permeability model. Can. Geotech. J., 54, 11, 1537–1552. DOI: 10.1139/cgj-2016-0629

Shao, W., Yang, Z., Ni, J., Su, Y., Nie, W. and Ma, X.: 2018, Comparison of single- and dual-permeability models in simulating the unsaturated hydro-mechanical behavior in a rainfall-triggered landslide. Landslides, 15, 12, 2449–2464. DOI: 10.1007/s10346-018-1059-0

Shuin, Y., Hotta, N., Suzuki, M., Ogawa and K. Ichiro: 2012, Estimating the effects of heavy rainfall conditions on shallow landslides using a distributed landslide conceptual model. Phys. Chem. Earth, 49, 44–51. DOI: 10.1016/j.pce.2011.06.002

Šimůnek, J., Jarvis, N.J. Van Genuchten, M.T. and Gärdenäs, A.: 2003, Review and comparison of models for describing non-equilibrium and preferential flow and transport in the vadose zone. J. Hydrol., 272, 1–4, 14–35. DOI: 10.1016/S0022-1694(02)00252-4

Wang, H., Jiang, Z., Xu, W., Wang, R. and Xie, W.: 2022, Physical model test on deformation and failure mechanism of deposit landslide under gradient rainfall. Bull. Eng. Geol. Environ., 81, 66. DOI: 10.1007/s10064-021-02566-y

Wang, Z., Timlin, D., Kouznetsov, M., Fleisher, D., Li, S., Tully, K. and Reddy, V.: 2020, Coupled model of surface runoff and surface-subsurface water movement. Adv. Water Resour., 137, December 2019, 103499. DOI: 10.1016/j.advwatres.2019.103499

Wu, L.Z., Huang, R.Q., Xu, Q., Zhang, L.M., and Li, H.L.: 2015, Analysis of physical testing of rainfall-induced soil slope failures. Environ. Earth Sci., 73, 12, 8519–8531. DOI: 10.1007/s12665-014-4009-8

Wu, Y.S., Liu, H.H. and Bodvarsson, G.S.: 2004, A triple-continuum approach for modeling flow and transport processes in fractured rock. J. Contam. Hydrol., 73, 1–4, 145–179. DOI: 10.1016/j.jconhyd.2004.01.002

Yu, M., Van Der Ploeg, M., Lwanga, E.H., Yang, X., Zhang, S., Ma, X., Ritsema, C.J. and Geissen, V.: 2019, Leaching of microplastics by preferential flow in earthworm (Lumbricus terrestris) burrows. Environ. Chem., 16, 1, 31–40. DOI: 10.1071/EN18161

Zhang, L.M., Zhang, S. and Huang, R.Q.: 2014, Multi-hazard scenarios and consequences in Beichuan, China: The first five years after the 2008 Wenchuan earthquake. Eng. Geol., 180, 4–20. DOI: 10.1016/j.enggeo.2014.03.020

Zhang, Y., Zhang, Z., Ma, Z., Chen, J., Akbar, J., Zhang, S., Che, C., Zhang, M. and Cerdà, A.: 2018, A review of preferential water flow in soil science. Can. J. Soil Sci., 98, 4, 604–618. DOI: 10.1139/cjss-2018-0046

Zhu, Y. and Xiao, Y.: 2020, Slope stability from a hydrological perspective : taking typical soil slope as an example. Adv. Civ. Eng., 2, 1-17. DOI: 10.1155/2020/1273603

Zhu, Y., Ishikawa, T., Siva Subramanian, S. and Luo, B.: 2020, Simultaneous analysis slope ,instabilities on a small catchment-scale using coupled surface and subsurface flows. Eng. Geol., 275, 105750. DOI: 10.1016/j.enggeo.2020.105750